Controllable Fabrication and Rectification of Bipolar Nanofluid Diodes in Funnel-Shaped Si_3N_4 Nanopores

Lei, Xin; Zhang, Jiayan; Hong, Hao; Wei, Jiangtao; Liu, Zewen; Jiang, Lei

DOI
10.1002/smll.202303370

Publication date
2023

Document Version
Final published version

Published in
Small

RESEARCH ARTICLE

NANO · MICRO small
www.small-journal.com

Controllable Fabrication and Rectification of Bipolar Nanofluid Diodes in Funnel-Shaped Si_3N_4 Nanopores

Xin Lei, Jiayan Zhang, Hao Hong, Jiangtao Wei, Zewen Liu, and Lei Jiang**

Solid-state nanopores attract widespread interest, owning to outstanding robustness, extensive material availability, as well as capability for flexible manufacturing. Bioinspired solid-state nanopores further emerge as potential nanofluidic diodes for mimicking the rectification progress of unidirectional ionic transport in biological K^+ channels. However, challenges that remain in rectification are over-reliance on complicated surface modifications and limited control accuracy in size and morphology. In this study, suspended Si_3N_4 films of only 100 nm thickness are used as substrate and funnel-shaped nanopores are controllably etched on that with single-nanometer precision, by focused ion beam (FIB) equipped with a flexibly programmable ion dose at any position. A small diameter 7 nm nanopore can be accurately and efficiently fabricated in only 20 ms and verified by a self-designed mathematical model. Without additional modification, funnel-shaped Si_3N_4 nanopores functioned as bipolar nanofluidic diodes achieve high rectification by simply filling each side with acidic and basic solution, respectively. Main factors are finely tuned experimentally and simulatively to enhance the controllability. Moreover, nanopore arrays are efficiently prepared to further improve rectification performance, which has great potential for high-throughput practical applications such as extended release of drugs, nanofluidic logic systems, and sensing for environmental monitoring and clinical diagnosis.

1. Introduction

Nanopores were first used as molecular sensors for polynucleotide detection in 1996.[1] Since then, solid-state nanopores have emerged as a highly stable platform, offering mechanical robustness, flexible surface modification, and adaptability for extended applications such as protein detection,[2] DNA sequencing,[3] drug screening,[4] water purification,[5] and ion logic circuits.[6] Inspired by the natural ion channels embedded in cell membranes, biomimetic solid-state nanopores and nanochannels with smart function, such as selective transportation,[7] controllable gating,[8] and ionic rectification,[9] have attracted wide attention in the past decades. For example, an inwardly rectified K^+ channel carried more inward ion current than reverse ion current,[10] which dominated the ion flow direction. The outstanding ionic current rectification (ICR) property could be emulated through the use of artificial solid-state nanopores and nanochannels, also known as a nanofluidic diode. By applying a bias voltage to the nanopore through two unpolarized electrodes placed on either side of the nanopore, the electric field drove an asymmetric migration of anions and cations in solution, producing an asymmetric current-voltage (I-V) curve. Currently, there are three types of nanopores with rectification function. The first type has an asymmetric geometry and a uniform surface charge distribution,[11] typically a conical-shaped polyethylene terephthalate (PET) nanochannel/nanopore. By fine-tuning the geometrical properties, the symmetry of electric potential in nanopore was broken and the ion trap was created,[12] leading to a closed state of the ion current at one-way voltage. The second type of rectified nanopores is mainly dominated by asymmetric surface charge distribution.[13] In addition, other types of nanopores that can also generate ICR, such as a symmetric nanopore with different electrolyte solutions at two sides[14] or a metal oxide layer with an asymmetric vacancy

X. Lei, J. Zhang
School of Chemistry
Beihang University
Beijing 100191, P. R. China

X. Lei, H. Hong, J. Wei, Z. Liu
School of Integrated Circuits
Tsinghua University
Beijing 100084, P. R. China
E-mail: liuzw@tsinghua.edu.cn

H. Hong
Department of Microelectronics
Delft University of Technology
Delft 2628 CD, The Netherlands

L. Jiang
Key Laboratory of Bio-Inspired Materials and Interfacial Science
Technical Institute of Physics and Chemistry
Chinese Academy of Sciences
Beijing 100190, P. R. China
E-mail: jianglei@iccas.ac.cn

L. Jiang
School of Future Technology
University of Chinese Academy of Sciences
Beijing 101407, P. R. China

The ORCID identification number(s) for the author(s) of this article can be found under https://doi.org/10.1002/smll.202303370

DOI: 10.1002/smll.202303370

distribution inside it.[15] Initially, rectification could be realized by combining different nanopore regions of the same polarity but varying charge densities. To reach an enhanced ICR, Daiguji first proposed a rectified nanopore with opposite surface charges on each side, called a bipolar nanofluidic diode/transistor.[16] Later, bipolar nanofluidic diodes were further developed to form controllable gating systems by asymmetrically modification of environmental-responsive molecules on the nanopore surface, such as pH-responsive molecules,[17] photo-responsive molecules,[18] ion-responsive molecules,[19] and temperature-responsive molecules.[20] One typical experiment was performed in a cigar-shaped nanochannel based on asymmetric modification of pH response in each tip.[21] Turning the pH on both sides of the nanopore allowed the flexibly switch between "on" and "off", respectively, which resulted in high-performance cooperative gating and high-efficiency ionic rectification.

However, the existing nanochannels with rectification rely too heavily on elaborate chemical modifications, leading to an overuse of polymers, typically thicker PET membranes. Besides, the multilayer structure of the membrane induces erratic etching rates in different layers, which results in surface roughness and limited control accuracy of size and morphology.[22] Meanwhile, the simulation results illustrate that a nanopore tip with only a few hundred nanometers in length is sufficient for ionic rectification, without the excessively thick films.[23] In this work, a suspended silicon nitride film with thickness of only 100 nm is chosen as the substrate to experimentally demonstrate the existence of rectification. Funnel-shaped nanopores with bipolar nanofluid diode behavior are controllably fabricated on that film by focused ion beam (FIB) with single-nanometer precision. A mathematical model based on the funnel-shaped nanopores was built to accurately predict the through-hole current and the critical dimension. Furthermore, solid-state nanopore arrays were efficiently prepared to improve the rectification performance. In particularly, the funnel-shaped Si_3N_4 nanopore could natively achieve bipolar pH-response on the cylindrical side and the conical side, respectively, without additional modification processes. Last but not least, the main factors affecting the rectification ratio were also studied and classified to further improve the controllability of rectification.

2. Results and Discussion

2.1. Controllable Fabrication of Funnel-Shaped Nanopores

As shown in **Figure 1**a, we first prepare a suspended silicon nitride membrane with thickness of only 100 nm and size of 100 μm × 100 μm using multi-step Micro-Electromechanical Systems (MEMS) processes. Next, funnel-shaped nanopores with bipolar nanofluid diode behavior are fabricated on that film by a two-step FIB etching technique with a programmable ion-dose editor at any position as shown in Figure 1b. Applying this editor, the ion dose is first distributed in a circular shape and increased in a linear gradient from edge to center (from 0 to 1.5 nC μm^{-2}), so that a conical blind pore is pre-etched on the nanofilm. Second, the ion dose is concentrated at the center, and the cylindrical through hole is engraved to form a complete funnel-shaped nanopore. Furthermore, by fine-tuning the maximum dose of the conical pore from 0.5 to 3.5 nC μm^{-2}, the depth of the conical pore linearly rises from 14 to 100 nm and reaches the perforation threshold at 2.1–2.4 nC μm^{-2} in Figure 1c. On the basis of the conical blind pore, the etching time of the cylindrical part is attentively adjusted by steps of 10 ms to produce a funnel-shaped nanopore, as shown in Figure 1d. The pore diameter grows linearly from only 7 nm to more than 35 nm with the logarithm of etching time enabling single-nanometer size precision. Nanopores with diameters below 5 nm are further obtained by He^+ etching (see Figure S1, Supporting Information). The insets of front, side, and cross-section views precisely demonstrate the variation of pore size and morphology. Besides, ion dose can be accurately adjusted and edited as linear straight line, concave quadratic curve or convex quadratic curve, and strictly positioned and etched to form corresponding 3D patterns as cone, deep bowl, and slit pore respectively, in Figure S2 (Supporting Information). Taking advantage of single-nanometer etching accuracy (<3 nm for Ga^+), extremely high imaging resolution (0.5 nm for He^+), and smooth surface roughness (<0.5 nm), FIB can realize the controllable fabrication of micro-nano structures and outline delineation by programmable ion dose distribution. Moreover, the extremely high processing efficiency (only 20 ms for single nanopore) contributes to high-throughput preparation and application.

2.2. Electrical Test Platform and Mathematical Model

Figure 2a completely shows an electrical test platform based on solid-state nanopores. The funnel-shaped nanopore is the only channel for KCl solution to flow from one cell to the other for accurate detection of the through-nanopore current (see Methods for detailed current measurement). Inspired by the resistance model of cylindrical nanopores[24] and conical nanochannels,[25] the resistance model R based on funnel-shaped nanopore is initially constructed to accurately predict the through-pore current and the critical size, which is calibrated by I–V curve. Before test, the solution is adjusted to the equipotential point ($pH = 4.1$) [26] to make the Si_3N_4 surface uncharged, avoiding the influence of double electric layers. R is composed of the bulk resistance inside the nanopore [27] and the access resistance at the entrance,[28] as shown in Figure 2b:

$$R = R_{pore} + R_{acc} \tag{1}$$

R_{pore} and R_{acc} are defined by the dimensional parameters of cylinder part and cone part with solution resistivity ρ:

$$R_{pore} = R_{pore,\,\mathrm{con}} + R_{pore,\,\mathrm{cyl}} \tag{2}$$

$$R_{pore,\mathrm{cyl}} = \rho \frac{4L_{\mathrm{cyl}}}{\pi D_{\mathrm{cyl}}^2} \tag{3}$$

$$R_{pore,\,\mathrm{con}} = \rho \frac{4L_{\mathrm{con}}}{\pi D_{\mathrm{con}} D_{\mathrm{cyl}}} \tag{4}$$

$$R_{acc} = R_{acc,\,\mathrm{con}} + R_{acc,\,\mathrm{cyl}} \tag{5}$$

$$R_{acc,\,\mathrm{cyl}} = \rho \frac{1}{2D_{\mathrm{cyl}}} \tag{6}$$

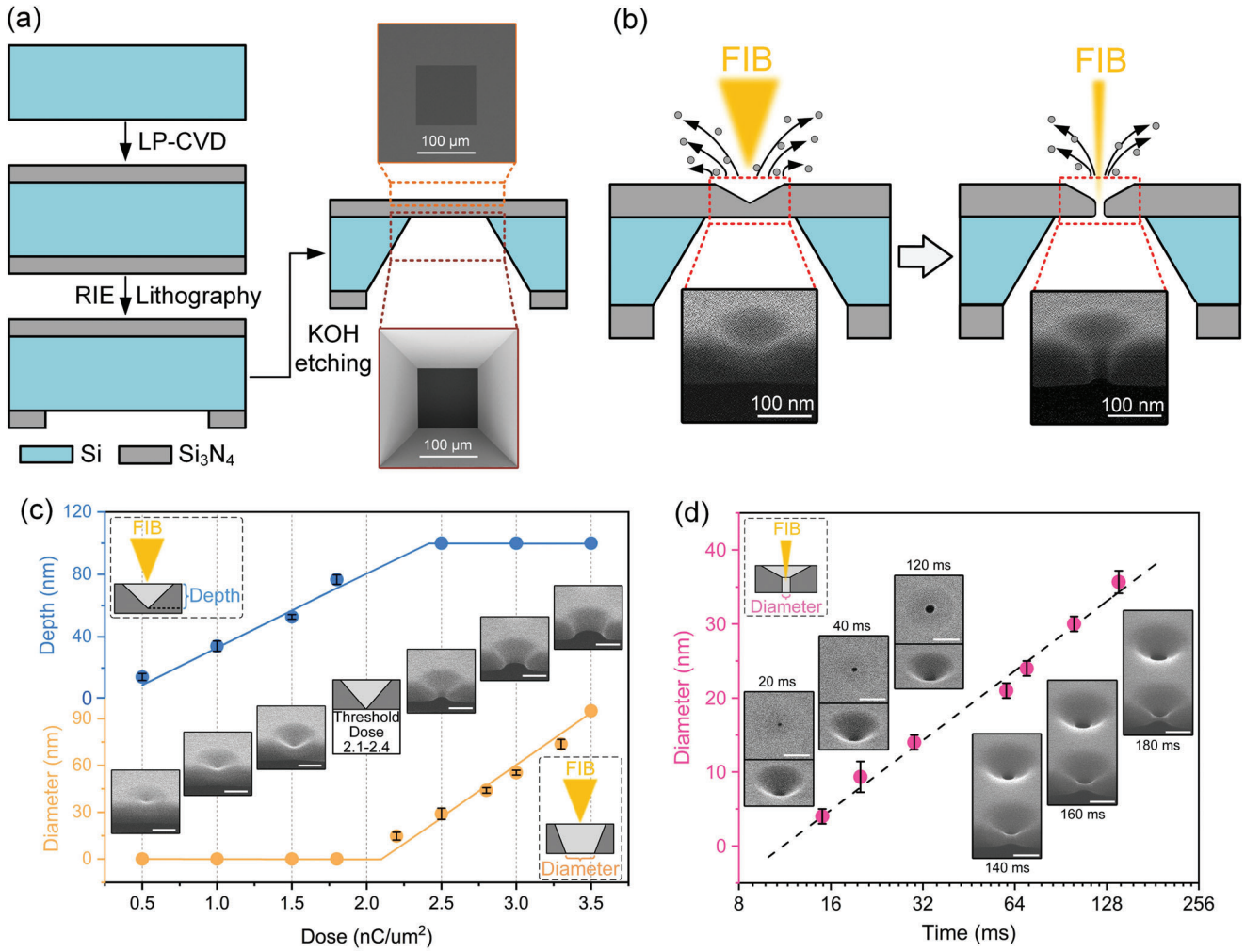

Figure 1. Controllable fabrication processes of silicon nitride nanofilm and funnel-shape nanopore. a) Silicon wafer with thickness of 200 μm (4-inch, N-type, 100) is used as the substrate; Si_3N_4 nanofilm with thickness of 100 nm is deposited on both sides of the silicon wafer by low pressure chemical vapor deposition (LP-CVD); the bottom surface of Si_3N_4 is patterned by photolithography and reactive ion etching (RIE), exposing the silicon window of 390 μm × 390 μm; The wafer is etched in 33 wt.% KOH solution at 80 °C for 3.5 h to remove the silicon behind the window thoroughly; after slicing and cleaning, a 100 μm × 100 μm suspended Si_3N_4 nanofilm is obtained. Two scanning electron microscope (SEM) images show the front and the back of the nanofilm. b) Two-step FIB etching is used to controllably fabricate the conical blind pore and the cylindrical through pore respectively, and finally combined to form the funnel-shaped nanopores. c) In the first step: cone-part nanopores with different depth and opening diameters are etched by changing the ion dose from 0.5 to 3.5 nC μm^{-2}. d) In the second step: cylinder-part nanopores with different diameters are etched by adjusting the etching time from 20 to 180 ms.

$$R_{acc,\ con} = \rho \frac{1}{2D_{con}} \tag{7}$$

Where $L_{cyl} = 50\ nm$ and $L_{con} = 50\ nm$ are the length of cylindrical part and conical part; $D_{cyl} = 16nm$ and $D_{con} = 150\ nm$ are the entrance diameter respectively; ρ is the reciprocal of conductivity σ. The specific dimensional positions are shown in Figure S3 (Supporting Information). We first utilize the theoretical model to estimate nanopore resistance, and the ion concentration ranges from 10^{-4} M ($\sigma = 2.70 \times 10^{-3}$ S/m) to 10 M ($\sigma = 1.12 \times 10^{2}$ S/m). It is obvious in Figure 2c that the resistance increases linearly from 2.77×10^{6} Ω to 1.15×10^{11} Ω as the concentration declines. This is highly consistent with previous results,[29] because the total amount of K^+ and Cl^- in lower concentration solutions is significantly reduced, resulting in a decrease in conductivity and a corresponding increase in resistance. The experimental data in same condition also proves that the test resistance linearly increases from 2.76×10^{7} Ω to 1.51×10^{10} Ω with the decrease of concentration, and the resistance results are well scattered around the fitting line, as shown in Figure 2c. Furthermore, when we adjust the diameter of cylinder part from 40 to 100 nm, model resistances (from 6.02×10^{6} Ω to 1.72×10^{6} Ω) are also highly coincident and experimental resistances (from 5.72×10^{6} Ω to 1.80×10^{6} Ω) as shown in Figure 2d. The graph also reveals that larger pore size is beneficial to conduction of K^+ and Cl^-, resulting in lower resistance. These findings indicate that the theoretical model can effectively predict the resistance of the funnel-shaped nanopore soaked in solution or, in reverse, to

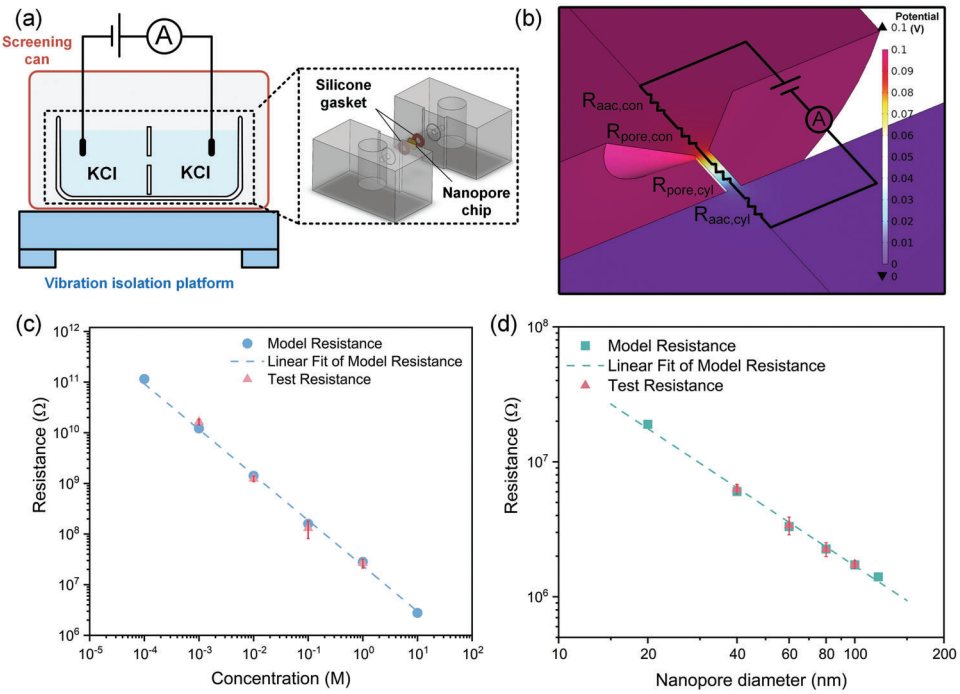

Figure 2. The electrical test platform based on solid-state nanopores and the resistance model for funnel-shaped nanopores. a) The nanopore membrane is sandwiched in the flow cell with silicone gaskets to form two half cells, to which a bias voltage is applied to test the through-pore current; A screening can and vibration isolation are used to prevent the impact of electromagnetic waves and external vibration. b) The nanopore resistance is composed of the bulk resistance and access resistance of the cylinder part and the cone part, respectively; the background shows the potential distribution of the nanopore platform after applying a bias voltage of 0.1 V. c) In tests and models, the logarithm of nanopore resistance reduces linearly with the increase in the logarithm of KCl concentration. d) In tests and models, the logarithm of nanopore resistance also reduces linearly with the increase in the logarithm of the nanopore diameter of cylinder part.

calculate the critical size. Last but not least, the bulk resistance in the cylinder part $R_{pore,cyl}$ has the highest proportion of the total resistance (80.3% in resistance model and 93.0% in simulation of 0.1 M KCl) shown in Table S1 (Supporting Information), which reveals that the marked reduction of potential mainly happens in the cylindrical section, as demonstrated in Figure 2b. The existence of the steep gradient in electric field is beneficial to the successful passage of nanoparticles through the nanopore sensor.[30]

2.3. Rectification based on Funnel-Shaped Nanopores

Figure 3a reveals that a funnel-shaped nanopore functions as a bipolar nanofluidic diode achieving high rectification ($ratio_{|_{l+1\ V}|/|_{l-1\ V}|} = 5$) by simply filling each side with acidic solution ($pH = 1$) and basic solution ($pH = 11.9$) in 0.01 M KCl to make the surfaces positively and negatively charged respectively. However, the funnel nanopore with uncharged surfaces is more like a fixed-resistance resistor with no rectification at all. The rectification effect is attributed to the presence of an electrical double layer (EDL) [31] on charged nanopore surface and the asymmetric distribution of K^+ and Cl^-.[12,32] To demonstrate the existence of the double layer and surface-charge-governed ion transport, the ionic conductance of nanopores at different concentrations is analyzed in detail, as shown in Figure S4 (Supporting Information).

Initially, when the cylindrical segment is negatively charged and the conical segment is positively charged, the K^+ and Cl^- gather on the respective surfaces to form an asymmetric EDL, as shown in Figure 3b. By applying a positive voltage, an abundance of K^+ in the cylinder and Cl^- in the cone accumulates toward the funnel center to form the high conductivity shown in Figure 3c–e. However, when the electric field is inverted, the ions are both far away from the center to create the cavity and low conductance results, as shown in Figure 3f–h. The apparent difference of conductivity at positive and negative voltages results in the macroscopic rectification. The same results are also verified in simulations, shown in Figure S5 (Supporting Information, see Methods for detailed simulation). Without doubt, heterogeneously charged nanopores induce ion aggregation and dispersion, respectively, achieving high rectification. Meanwhile, the asymmetric structure of the funnel shape with the same surface charges could also lead to an uneven distribution of homogeneous-charged ions on the nanopore surface and achieve weak rectification. However, when the nanopore surface is not charged without the EDL, K^+ and Cl^- are uniformly distributed everywhere in solution, resulting in no rectification effect. In a word, the asymmetric characteristic of the nanopore shape and charged surfaces gives rise to a non-uniform distribution and transport of anionic and cationic ions, which in turn generates the rectification effect. The non-uniform distribution of ions is mainly formed within the EDL,[] so the nanopore diameter should be as much as possible comparable to the thickness of the layer to maximize the rectification effect.[33] In particular, thanks to the presence of silanol groups and secondary

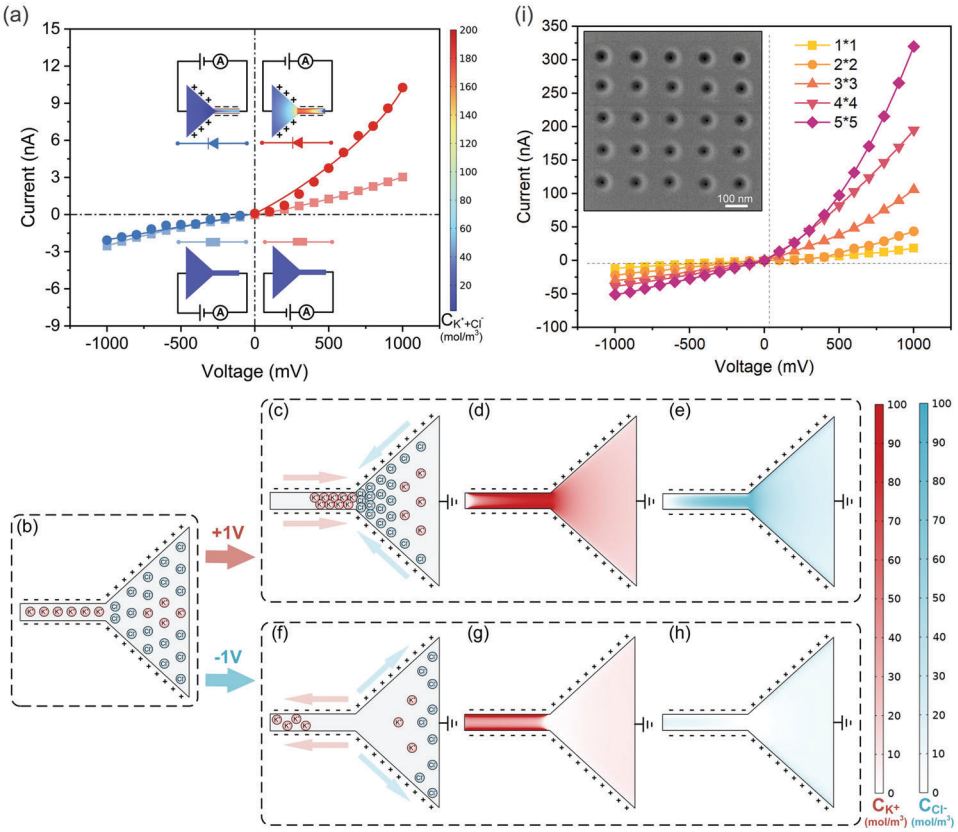

Figure 3. Rectification based on funnel-shaped nanopores. a) The asymmetric charged surface (+0.01 C m^{-2} in the conical part and −0.1 C m^{-2} in the cylindrical part) results in a high rectification effect as a diode; the uncharged surface leads to no rectification as resistance as shown in the experimental results and the simulation results shown in insets. b–h) The rectification principle of asymmetric charged funnel-shape nanopores. b) Initial ion distribution with the cylindrical part negatively charged and the conical part positively charged; c) under +1 V, ions converge to form high conductivity. d,e) Under +1 V, simulation results of the concentration distribution of K^+ and Cl^-, respectively. f) Under −1 V, ions disperse to form low conductivity. g,h) Under −1 V, simulation results of the concentration distribution of K^+ and Cl^-, respectively. i) Ionic current increases with the size of the nanopore array from 1 × 1 to 5 × 5, especially at positive voltages; the inset image is the 5 × 5 nanopore array of same diameter (10 nm). Detailed parameters of the nanopore and the solution in the experiment and the simulation are shown in Table S2 (Supporting Information).

amine groups on Si_3N_4 surfaces (the isopotential point, pH_{iep} = 4.1),[26] the surface charge density could be smoothly adjusted for the conical and cylindrical segments separately, by briefly immersion in different pH solutions, without the complicated modification process.[20] It is of great importance that the solution should be added in the cone side first to ensure forming the steep decrease of concentration at the narrowest junction of conical and cylindrical segment,[34] avoiding the miscibility of the two different solutions. This effective means of adding heterogeneous solutions to both sides for rectification is widely witnessed in cigar-shaped nanopores,[35] cone-shaped nanopores,[36] hourglass nanopores,[14] and other biomimetic smart nanoflow channels.

In addition, asymmetric concentrations of acids and bases can also have an effect on rectification. Specifically, when there is no concentration difference, the preferred direction of rectification is directed from the cylindrical section to the conical section as the negatively charged in cylindrical section and positively charged in conical section, as shown in Figure 3. After the addition of a tenfold concentration gradient (0.1 M acid in the conical section and 0.01 M base in the cylindrical section), diffusive ionic currents are introduced to influence the rectification. Due to the higher surface charge density and smaller diameter of the cylindrical section, the ion selectivity within the diffusive ion current is dominated by the negatively charged cylindrical section. Therefore, the diffusive ion flow from the high concentration side (cone section) is predominantly K^+, which is in the opposite direction to the original rectification. In conclusion, the concentration gradient introduced by the acid and base slightly reduces the rectification ratio. However, a greater concentration difference (100 times more) is required so that the ionic current is dominated by the diffusion current. At the same time, the presence of KCl will also somewhat weaken the effect of the concentration difference on the rectification.

Last but not least, based on the efficient fabrication by FIB, nanopore arrays of same diameter (10 nm) are efficiently prepared from 1 × 1 to 5 × 5 only in just 5 min. The increasing number of nanopores also leads to an increase in the ionic current, especially at positive voltages, which results in a steady linear raise in the rectification rate, as shown in Figure 3i and Figure S6 (Supporting Information). For our funnel-shaped nanopore array rectification, the diameter of the conical segment with the

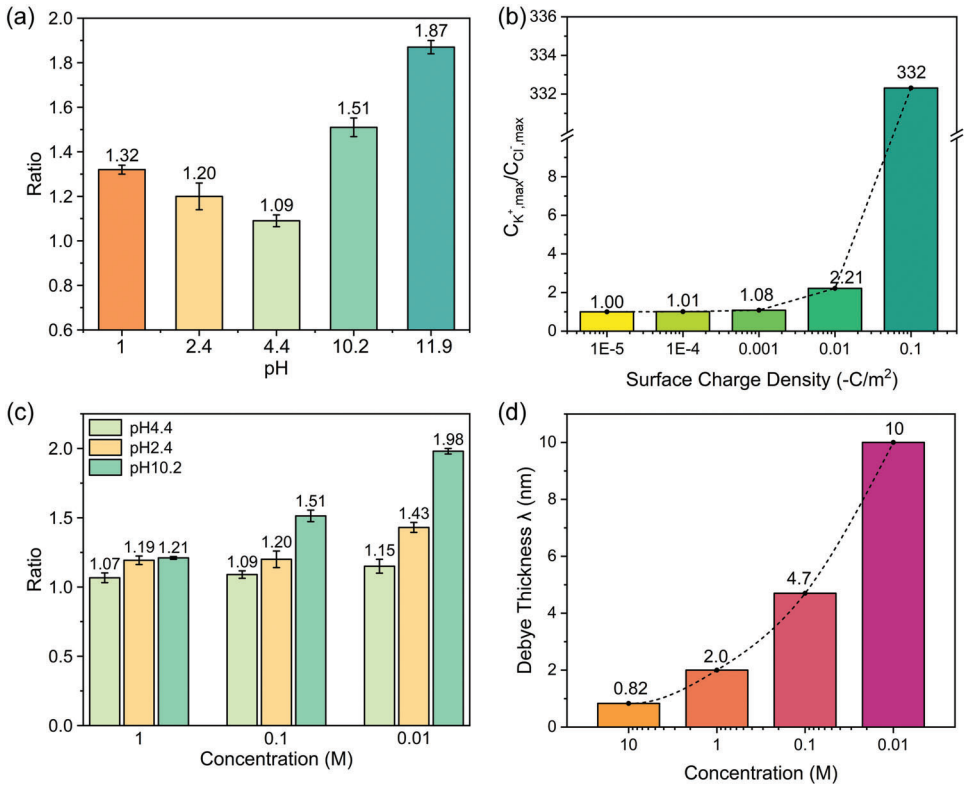

Figure 4. The effect of solution properties on nanopore rectification. a) The variation of rectification ratio is experimentally analyzed by changing the pH from 1 to 11.9. b) The effect of surface charge density growth from -10^{-5} to -0.1 C m^{-2} on the concentration ratio of K^+ and Cl^- in the nanopore surface, based on simulation results. c) The effect of KCl concentration (0.01, 0.1, and 1 M) on rectification at different pH's (2.4, 4.4, and 10.2) are compared experimentally. d) The variation of the extended EDL thickness at different concentrations from 0.01 to 10 M is obtained from simulation results. Detailed parameters of the nanopore and the solution in the experiment and the simulation are shown in Table S2 (Supporting Information).

large opening (100 nm) is 10 times larger than the diameter of the cylindrical segment with the small opening (10 nm), resulting in the spacing between conical segments of adjacent nanopores being much smaller than the cylindrical segments. As a result, the stronger pore-pore interactions in the conical segment leads to ion sharing and lower ion concentration at the pore opening.[37] However, the cylindrical segments of adjacent nanopores are farther apart with less change in concentration. Therefore, a certain concentration difference arises between the two sides of the nanopore. Due to the higher negative charge of the cylindrical segments, K^+ passes preferentially through the nanopore and the current direction caused by the concentration difference coincides with the initial rectification conduction direction. This enhances the rectification effect. So, as the number and density of nanopores increases, the concentration difference is further enhanced and the rectification rate is further elevated. This facilitates further exploration of high-throughput functions and applications such as nanosensors,[38] nanoreactors,[39] and energy conversion and storage.[40]

2.4. Effect of Solution Properties on Rectification

To further understand the effect of solution properties on rectification, we first investigate the key factors in solution, in particular pH and KCl concentration. Both sides of the nanopore are filled with solutions of identical conditions to precisely characterize the rectification effect. At $pH = 4.4$, the Si_3N_4 nanopore maintains the minimum rectification ratio of about 1.09, due to the almost uncharged surface near the isopotential point ($pH_{iep} = 4.1$), as shown in **Figure 4**a. However, the rectification ratio rises to 1.32 and 1.87 when the pH decreases to 1 or increases to 11.9, respectively. This is attributed to the presence of silanol and amine groups on the Si_3N_4 surface, providing a negatively or positively charged barrier at different pH values through dissociation or association reactions with surface protons, respectively.[26] And the surface charge density increases with further ramping up of acidity and alkalinity, which causes enhanced rectification. For further proof, we simulate the ion distribution within the nanopore at different surface charge densities, from -10^{-5} to -10^{-1} C m^{-2}, as shown in Figure 4b and Figure S7a (Supporting Information). When approaching the negatively charged pore wall, the concentration of K^+ within the EDL is significantly higher than that of Cl^-. And as the surface charge density increases, the concentration ratio of K^+ to Cl^- in the wall jumps from 1:1 to 332:1 wonderfully. This demonstrates that the growing surface charge density yields a higher and purer concentration of counter ions within the EBL, which contributes to the intensive rectification and ion selectivity. Secondly, the effect of KCl concentration (0.01, 0.1, and 1 M) on rectification at different pH's is compared, as

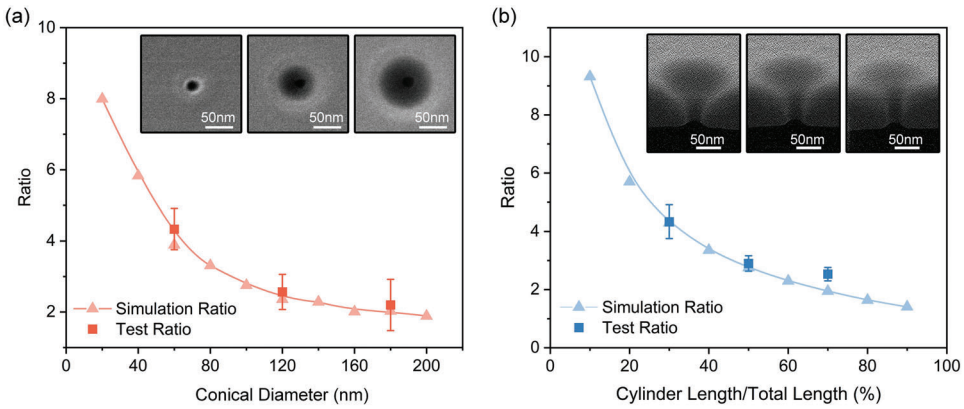

Figure 5. Effect of nanopore size on rectification. a) The smaller the opening diameter in the conical side, the higher the rectification ratio; the experimental results and the simulation results remain consistent; Inset images of three different opening diameter nanopores. b) The lower the length ratio on the cylindrical side, the higher the rectification ratio; the experimental results and the simulation results remain consistent; inset images of three different length ratio nanopore. Detailed parameters of the nanopore and the solution in the experiment and the simulation are shown in Table S2 (Supporting Information).

shown in Figure 4c. When the surface is electrically neutral at $pH = 4.4$, the double layer is not present and there is slight rectification ($ratio = 1.1$) despite changing the concentration. However, under acidic ($pH = 2.4$) and alkaline ($pH = 10.2$) conditions, the recovery of the surface charge and the double layer leads to a remarkable improvement in rectification ratio. In particular, the increasing rate of rectification becomes more pronounced at lower concentration, typically rising from 1.1 to 1.98 at 0.01 M. To explain this phenomenon, the ion distribution within the nanopore was also simulated at concentrations from 0.01 to 10 M, as shown in Figure 4d and Figure S7b (Supporting Information). The results clearly reveal that the concentration mainly affects the thickness of the extended EDL (the thickness where the concentration of K^+ is higher than that of Cl^- starting from the pore wall), which increases significantly with lower concentration. At 10 M, the thickness of the layer is only 0.82 nm which contributes negligibly to the rectification in a 10 nm-radius nanopore. However, when the ion concentration is reduced to 0.01 M, the thickness increases dramatically to 10 nm, comparable to the radius, which facilitates the asymmetric ion distribution and rectification within the funnel-shaped nanopore. The more dilute the electrolyte is, the thinner the resistant capability of the counter ions and thus the thicker the EDL.[41] And rectification relies on matching the thickness of EDL with the diameter of nanopore, so the concentration affects rectification by altering the thickness of EDL in turn.

2.5. Effect of Nanopore Size on Rectification

The effect of variable pore size on rectification in the funnel-shaped nanopore is further investigated experimentally and analyzed by simulation. Funnel pores of different opening diameters (conical diameter) and length ratios (cylinder length/total length) are precisely prepared and tuned by the FIB dose editor with single nanometer precision, as shown in the insets of **Figure 5**. At first, simulation results suggest that the reduction of the opening diameter from 200 to 20 nm facilitates the growth of the rectification ratio from 2 to 8, as shown in Figure 5a. Meanwhile, nanopores prepared from FIB with openings of 180, 120, and 60 nm are measured in experiments, where the rectification ratio grows from 2 to 2.5 and 4.5 respectively, all in the vicinity of the simulated fitting curve. Because of the heterogeneous charge on the conical and cylindrical sides, the narrower opening diameter is approaching the thickness of the EDL, which further enhances the asymmetric ion distribution on both sides of the nanopore and thus improves the rectification effect.[42] Then, we compare the effect of the length ratio between the conical part and the cylindrical part on rectification. The simulation results illustrate that as the length ratio of the cylindrical section decreases from 90% to 10% (total length 100 nm), the rectification ratio improves from 2 to 9.5, as shown in Figure 5b. The same trend is also observed experimentally where the rectification ratio rises from 3 to 4.5 as the length of the nanopore cylindrical section reduces from 70% to 30%. We use the classic "Trap" theory to further explain this phenomenon.[12] For nanopore with asymmetrical shape or asymmetric surface charges, the shape of the internal potential has been shown to be asymmetrical and toothed, reminiscent of the shape of a ratchet potential, if no voltage is applied externally, as shown in Figure S8a–d (Supporting Information). The minimum potential value is located at the tip of the nanopore. As shown in Figure S8b–e (Supporting Information), we can obtain the resulting potential curves of both polarity of the applied voltage, assuming that the externally applied voltage is simply superimposed with the internal electric field. Figure S8c (Supporting Information) shows that for a positive voltage, a trap of static power is created, resulting in a "close" state (low conductivity) of the pores. In Figure S8f (Supporting Information), applying a voltage of opposite polarity does not result in the formation of a trap and the ionic current is high. Further simulation results show that when a forward voltage of 1000 mV is applied to a cylindrical section with a length ratio of only 10%, the internal electric field of the nanopore in the direction of the axis creates a "Trap", which causes the passage of ions to be blocked, resulting in a low conductance in Figure S8g (Supporting Information). When the bias is reversed, the conductivity is high in Figure S8g (Supporting Information), together resulting in a high rectification ratio. However, when the length of the cylindrical section is

increased to 90%, the "trap" phenomenon decreases, resulting in a lower current difference between positive and negative bias, and thus a lower rectification, as shown in Figure S8i,j (Supporting Information). In summary, the presence of the "trap" at lower length ratio and positive voltages results in lower currents and higher rectification ratios. There is ample evidence that smaller opening sizes and a lower proportion of cylindrical segment are beneficial for higher rectification rates.

Last but not least, the stability of ionic rectification should be tested. We have therefore placed the nanopore under cyclic bias (from −1 to +1 V) and tested it for twelve consecutive cycles. The data is divided into four groups with three data points in each group, as shown in Figure S9a–d (Supporting Information), which demonstrate their IV curves. Their rectification trends are generally consistent, being in the cut-off state at negative voltages and in the on state at positive voltages. Then, Figure S9e (Supporting Information) provides statistics on their rectification ratios and the average rectification ratio for each group. As the number of cycles increased, the rectification ratio of the nanopores was basically stable and showed a small downward trend. after 12 cycles, the rectification ratio decreased slightly from 4.2 to 3.75, accounting for 89.3% of the initial rectification ratio. This is acceptable as the usual nanopore rectification test does not test for so many cycles.

However, the gradual decrease in the rectification ratio indicates that the miscibility of both sides of the solution, especially the miscibility of hydrogen and hydroxide ions, leads to a non-uniform charge distribution on the surface of the nanopore, especially near the pore intersection. Furthermore, the rectification change from the group 1 to the group 2 (91.9%) is more pronounced compared to the change in the group 3 (90.2%) and group 4 (89.3%). This could mean that miscibility is more pronounced in the initial few cycles then gradually slows down. To further illustrate the extent of non-uniform charge distribution, simulations were carried out. Detailed simulation results and analysis show in the supplementary material of Figure S10 (Supporting Information).

3. Conclusions

In conclusion, FIB etching with single-nanometer precision is developed to fabricate funnel-shaped Si_3N_4 nanopores of controllable size and shape with rectification behavior. Nanopores as small as 7 nm in diameter could be manufactured accurately and efficiently in just 20 ms and are validated by a self-designed mathematical model. Without additional or complex modification processes, funnel-shaped Si_3N_4 nanopores behave as pH-response bipolar nanofluidic diodes, achieving higher rectification (*ratio* = 5) by briefly filling each side with acidic and basic solution to make the surfaces positively and negatively charged, respectively. Particularly, finite-element simulations of the presence of the EDL and the asymmetric distribution of K^+ and Cl^- on the nanopore surface offers powerful evidence on the origin of ionic rectification, and is highly consistent with the laboratory observation. Therefore, rectification can be finely tuned by controlling the pH and KCl concentration of the solution to influence the surface charge density and EDL thickness, respectively. Meanwhile, a smaller opening diameter on the conical side and a lower length ratio of the cylindrical side can further improve the rectification effect. As a highly controllable, efficient and stable Si_3N_4 solid-state nanopore platform, the high-throughput nanopore array, as a bipolar nanofluid diode with tremendous performance, have shown great potential in practical applications, such as selective transport and separation of ions and molecules, controllable gating, clean energy conversion, and sensing. Moreover, with the development of techniques such as electron beam lithography (EBL), focused ion beam, and dielectric breakdown, nanopores and nanochannels of different shapes at sub-10 nm or even sub-nanometer scale can be readily prepared in inorganic materials, making them ideal models for the study of sub-continuous ion transport behavior.

4. Experimental Section

Characterization: The thickness of the suspended silicon nitride nanofilm was measured by ellipsometry (TPY-1, wavelength 632.8 nm). Forward and reverse imaging of the silicon nitride film was carried out with a scanning electron microscope (Zeiss, Gemini 300). The nanopore and its cross-section were etched in Si_3N_4 nanofilms using Ga^+ source in focused ion beam (Zeiss, Orion NanoFab). The FIB accelerating voltage was 30 kV, the ion beam current was 2 pA. Real-time changes of nanopore size and morphology during processing were observed by He^+ source focused ion beam.

Current Measurement: Before testing, the nanopore chip was thoroughly cleaned in piranha solution (H_2SO_4: H_2O_2 = 3:1 volume/volume) at 80 °C for 45 min to improve its hydrophilicity. It was sandwiched in the poly-tetra-fluoroethylene flow cell with silicone gaskets to form two half cells separated by the nanopores. Then, Ag/AgCl electrodes were used to connect the flow cell to the probe and link it to the patch clamp amplifier (Axopatch 200B, Molecular Devices Inc.) or the Keithley 2450 with the computer. Detailed parameters of the nanopore and the solution are shown in Table S2 (Supporting Information).

Simulation: The coupled Poisson-Nernst-Planck (PNP) and Navier-Stocks (NS) equations [43] were calculated. The default funnel-shaped nanopore model was designed so that the opening diameters of the conical and cylindrical sides were 100 and 10 nm respectively, and the lengths of both sides were 50 nm, which were then connected to a pair of cylindrical fluid cells with a length of 250 nm and a radius of 250 nm. It was a 2D-axisymmetric geometry that could be revolved about the axis to produce full 3D solutions. The default surface charge density was −0.1 and +0.01 C m^{-2} for the cylindrical and conical sides respectively. The 0.1 nm triangular grid was applied to the charged surface and the rest of the grid was generated by the system. The computation domain was assumed to be a room-temperature aqueous KCl solution, for which the following parameters were used: T = 298.15 K, the diffusion coefficient $D(K^+) = 1.956 \times 10^{-9}\ m^2/s$, $D(Cl^-) = 2.031 \times 10^{-9}\ m^2/s$,[44] and the relative dielectric constant $\varepsilon = 78.351$.[44] The default voltage difference between the two liquid cells was ±1000 mV. In order to obtain the ion current in the middle section of the nanopore in the COMSOL simulation, the following formula was used to calculate the ion current: $I = N_A \times e \int (J_{K^+} - J_{Cl^-})\, dS$. Where N_A is the Avogadro constant, e is the amount of charge per electron, J_{K+} and J_{Cl^-} are the fluxes of potassium ions and chloride ions respectively, and S is the middle cross section of the nanopore.

Supporting Information

Supporting Information is available from the Wiley Online Library or from the author.

Acknowledgements

This research was supported by Beijing Innovation Center for Future Chips, Beijing National Research Center for Information and The National Key R&D Program (2019YFA0707002).

Conflict of Interest

The authors declare no conflict of interest.

Author Contributions

X.L., J.Y.Z., and H.H. contributed equally to this work. X.L. and L.J. had the idea for the article. X.L., J.Y.Z., and H.H. performed the search and data analysis. X.L. wrote the initial drafts of the work. Z.W.L. and L.J. discussed the results and commented on the manuscript. All authors read and approved the final manuscript. X.L., J.Y.Z., and H.H. contributed equally to this work.

Data Availability Statement

The data that support the findings of this study are available from the corresponding author upon reasonable request.

Keywords

bipolar nanofluid diodes, current rectification, focus ion beam, Si_3N_4 nanopores, solid-state nanopores

Received: April 21, 2023
Revised: June 9, 2023
Published online: July 7, 2023

[1] J. J. Kasianowicz, E. Brandin, D. Branton, D. W. Deamer, *Proc. Natl. Acad. Sci. U.S.A.* **1996**, *93*, 13770.
[2] H. Ouldali, K. Sarthak, T. Ensslen, F. Piguet, P. Manivet, J. Pelta, J. C. Behrends, A. Aksimentiev, A. Oukhaled, *Nat. Biotechnol.* **2020**, *38*, 176.
[3] S. J. Heerema, L. Vicarelli, S. Pud, R. N. Schouten, H. W. Zandbergen, C. Dekker, *ACS Nano* **2018**, *12*, 2623.
[4] B. I. Karawdeniya, Y. N. D. Bandara, J. W. Nichols, R. B. Chevalier, J. R. Dwyer, *Nat. Commun.* **2018**, *9*, 3278.
[5] M. E. Warkiani, A. A. S. Bhagat, B. L. Khoo, J. Han, C. T. Lim, H. Q. Gong, A. G. Fane, *ACS Nano* **2013**, *7*, 1882.
[6] V. V. R. Nandigana, K. Jo, A. Timperman, N. R. Aluru, *Sci. Rep.* **2018**, *8*, 13941.
[7] Z. Xu, Z. P. Zhu, N. Li, Y. Tian, L. Jiang, *ACS Nano* **2018**, *12*, 10000.
[8] F. Xia, W. Guo, Y. D. Mao, X. Hou, J. M. Xue, H. W. Xia, L. Wang, Y. L. Song, H. Ji, O. Y. Qi, Y. G. Wang, L. Jiang, *J. Am. Chem. Soc.* **2008**, *130*, 8345.
[9] C. Y. Lin, L. H. Yeh, J. P. Hsu, S. Tseng, *Small* **2015**, *11*, 4594.
[10] D. Bichet, F. A. Haass, L. Y. Jan, *Nat. Rev. Neurosci.* **2003**, *4*, 957.
[11] G. Perez-Mitta, J. S. Tuninetti, W. Knoll, C. Trautmann, M. E. Toimil-Molares, O. Azzaroni, *J. Am. Chem. Soc.* **2015**, *137*, 6011.
[12] Z. S. Siwy, *Adv. Funct. Mater.* **2006**, *16*, 735.
[13] K. Xiao, G. H. Xie, Z. Zhang, X. Y. Kong, Q. Liu, P. Li, L. P. Wen, L. Jiang, *Adv. Mater.* **2016**, *28*, 3345.
[14] Z. Q. Li, Y. Wang, Z. Q. Wu, M. Y. Wu, X. H. Xia, *J. Phys. Chem. C* **2019**, *123*, 13687.
[15] a) Z. Q. Wu, C. Y. Li, X. L. Ding, Z. Q. Li, X. H. Xia, *J. Phys. Chem. Lett.* **2022**, *13*, 5267; b) Y. D. Kim, S. Choi, A. Kim, W. Lee, *ACS Nano* **2020**, *14*, 13727.
[16] H. Daiguji, Y. Oka, K. Shirono, *Nano Lett.* **2005**, *5*, 2274.
[17] M. Y. Liu, H. C. Zhang, K. Li, L. P. Heng, S. T. Wang, Y. Tian, L. Jiang, *Adv. Funct. Mater.* **2015**, *25*, 421.
[18] L. P. Wen, X. Hou, Y. Tian, F. Q. Nie, Y. L. Song, J. Zhai, L. Jiang, *Adv. Mater.* **2010**, *22*, 1021.
[19] Y. F. Wu, D. Y. Wang, I. Willner, Y. Tian, L. Jiang, *Angew. Chem.* **2018**, *57*, 7790.
[20] X. Hou, F. Yang, L. Li, Y. L. Song, L. Jiang, D. B. Zhu, *J. Am. Chem. Soc.* **2010**, *132*, 11736.
[21] H. C. Zhang, X. Hou, L. Zeng, F. Yang, L. Li, D. D. Yan, Y. Tian, L. Jiang, *J. Am. Chem. Soc.* **2013**, *135*, 16102.
[22] H. Mukaibo, L. P. Horne, D. Park, C. R. Martin, *Small* **2009**, *5*, 2474.
[23] X. W. Wang, J. M. Xue, L. Wang, W. Guo, W. M. Zhang, Y. G. Wang, Q. Liu, H. Ji, Q. Y. Ouyang, *J. Phys. D: Appl. Phys.* **2007**, *40*, 7077.
[24] a) S. W. Kowalczyk, A. Y. Grosberg, Y. Rabin, C. Dekker, *Nanotechnology* **2011**, *22*, 315101; b) M. Tsutsui, A. Arima, K. Yokota, Y. Baba, T. Kawai, *Sci. Adv.* **2022**, *8*, 8.
[25] K. Xiao, G. H. Xie, P. Li, Q. Liu, G. L. Hou, Z. Zhang, J. Ma, Y. Tian, L. P. Wen, L. Jiang, *Adv. Mater.* **2014**, *26*, 6560.
[26] K. B. Lin, Z. W. Li, Y. Tao, K. Li, H. J. Yang, J. Ma, T. Li, J. J. Sha, Y. F. Chen, *Langmuir* **2021**, *37*, 10521.
[27] R. W. Deblois, C. P. Bean, *Rev. Sci. Instrum.* **1970**, *41*, 909.
[28] J. E. Hall, *J. Gen. Physiol.* **1975**, *66*, 531.
[29] W. H. Guan, R. Fan, M. A. Reed, *Nat. Commun.* **2011**, *2*, 8.
[30] J. S. Zhou, Y. Q. Wang, L. D. Menard, S. Panyukov, M. Rubinstein, J. M. Ramsey, *Nat. Commun.* **2017**, *8*, 8.
[31] R. B. Schoch, J. Y. Han, P. Renaud, *Rev. Mod. Phys.* **2008**, *80*, 839.
[32] Q. Liu, Y. Wang, W. Guo, H. Ji, J. Xue, Q. Ouyang, *Phys Rev E* **2007**, *75*, 6.
[33] M. L. Kovarik, K. M. Zhou, S. C. Jacobson, *J. Phys. Chem. B* **2009**, *113*, 15960.
[34] a) E. B. Kalman, I. Vlassiouk, Z. S. Siwy, *Adv. Mater.* **2008**, *20*, 293; b) I. Vlassiouk, Z. S. Siwy, *Nano Lett.* **2007**, *7*, 552.
[35] M. Ali, P. Ramirez, H. Q. Nguyen, S. Nasir, J. Cervera, S. Mafe, W. Ensinger, *ACS Nano* **2012**, *6*, 3631.
[36] S. Nasir, M. Ali, P. Ramirez, V. Gomez, B. Oschmann, F. Muench, M. N. Tahir, R. Zentel, S. Mafe, W. Ensinger, *ACS Appl. Mater. Interfaces* **2014**, *6*, 12486.
[37] L. X. Cao, Q. Wen, Y. P. Feng, D. Y. Ji, H. Li, N. Li, L. Jiang, W. Guo, *Adv. Funct. Mater.* **2018**, *28*, 8.
[38] M. F. Zhang, T. Chen, Y. K. Liu, J. L. Zhang, H. R. Sung, J. Yang, J. P. Zhu, J. Q. Liu, Y. C. Wu, *ACS Sens.* **2018**, *3*, 2446.
[39] L. Mi, J. C. Yu, F. He, L. Jiang, Y. F. Wu, L. J. Yang, X. F. Han, Y. Li, A. Liu, W. Wei, Y. J. Zhang, Y. Tian, S. Q. Liu, L. Jiang, *J. Am. Chem. Soc.* **2017**, *139*, 10441.
[40] H. P. Zhao, C. L. Wang, R. Vellacheri, M. Zhou, Y. Xu, Q. Fu, M. H. Wu, F. B. Grote, Y. Lei, *Adv. Mater.* **2014**, *26*, 7654.
[41] a) H. Daiguji, *Chem. Soc. Rev.* **2010**, *39*, 901; b) P. Zhang, M. Xia, F. W. Zhuge, Y. Zhou, Z. Y. Wang, B. Y. Dong, Y. Y. Fu, K. C. Yang, Y. Li, Y. H. He, R. H. Scheicher, X. S. Miao, *Nano Lett.* **2019**, *19*, 4279.
[42] W. Guo, Y. Tian, L. Jiang, *Acc. Chem. Res.* **2013**, *46*, 2834.
[43] I. Vlassiouk, S. Smirnov, Z. Siwy, *Nano Lett.* **2008**, *8*, 1978.
[44] L. H. Yeh, M. Zhang, S. W. Joo, S. Qian, *Electrophoresis* **2012**, *33*, 3458.